ELSEVIER

Polymer 43 (2002) 643–652

polymer

www.elsevier.com/locate/polymer

Monte Carlo simulations on filler-induced network chain deformations and elastomer reinforcement from oriented oblate particles ☆

M.A. Sharaf[a,*], J.E. Mark[b]

[a]Department of Chemistry, Helwan University, Ain-Helwan, Cairo 11795, Egypt
[b]Department of Chemistry and Polymer Research Center, The University of Cincinnati, Cincinnati, OH 45221-0172, USA

Abstract

Although the filler particles typically used to reinforce elastomers are at least approximately spherical, prolate (needle-shaped) or oblate (disc-shaped) particles have been used in some cases. The fact that anisotropic structures and properties can be obtained in these cases has encouraged a number of experimental and theoretical investigations. The present study extends some earlier Monte Carlo simulations on prolate particles in an amorphous polyethylene matrix, but now focuses on oblate particles. The particles were placed on a cubic lattice, and were oriented in a way consistent with their orientation in composites that were the subject of an experimental investigation by one of the authors. Rotational isomeric state representations of the chains were then generated to model the elastomeric network in the presence of the filler particles. The chain end-to-end distributions were found to be non-Gaussian, and to depend significantly on the excluded volumes of the particles. The particle-induced deformations of the network chains were consistent with results of some other relevant simulations and with recent neutron scattering results. Specifically, the chain dimensions were found to decrease with increase in the axial ratios characterizing the oblate shapes. As anticipated, the chain dimensions became anisotropic, with significant differences parallel and perpendicular to the direction of the particle axes. In general, the network chains tended to adopt more compressed configurations relative to those of prolate particles having equivalent sizes and aspect ratios. Use of these distributions in a standard molecular model for rubberlike elasticity gave values of the elongation moduli, and these were found to depend on the sizes, number, and axial ratios of the particles, as expected. In particular, the reinforcement from the oblate particles was found to be greatest in the plane of the particles, and the changes were in at least qualitative agreement with the corresponding experimental results.

Keywords: Monte Carlo methods; Rotational isomeric states (RIS); Reinforcement

1. Introduction

There is relatively little molecular understanding of the reinforcement of elastomers, even though this phenomenon is of extraordinary importance in the utilization of rubber-like materials [1–3]. The most common used reinforcing fillers are carbon black and silica, and they are typically separately prepared and then mechanically blended into an elastomer. Their importance is due to the fact that they can give large increases in the elastomeric modulus at a given strain, and improvements of various technically important properties such as tear and abrasion resistance, and resilience. The primary unagglomerated particles of the filler are almost always spherical by virtue of the way they are formed, for example in combustion processes or in precipitations from solution.

There have now been several studies showing that reinforcement of elastomers can also be achieved through the in-situ polymerization of monomers such as styrene to yield spherical particles of a glassy polymer, in this case polystyrene (PS) [4–6]. One advantage of such glassy particles is the fact that they can be deformed into non-spherical shapes through the deformation of the host elastomer above the glass transition of the PS, and then cooling the material under the applied deformation, before letting it relax [4–6]. In this way, biaxial deformations can be used to obtain oblate (disk-shaped) particles [6]. The same effect could be achieved by the use of uniaxial compression but with much greater difficulties in achieving significant uniform deformations. Such disc-like fillers could provide an interesting parallel to the clays platelets recently used to reinforce a variety of polymers, including elastomers.

The method described, however, also lines up the particles in the direction of the deformation used to distort the particles into their ellipsoidal shapes. In the case of oblate particles, the primary axis is perpendicular to the

☆ This paper was originally submitted to *Computational and Theoretical Polymer Science*. Following the incorporation of *Computational and Theoretical Polymer Science* into *Polymer*, this paper was consequently accepted for publication in *Polymer*.

* Corresponding author. Present address: School of Textiles and Fiber Engineering, Georgia Institute of Technology, Atlanta, GA 30332-0295, USA. Tel.: +1-404-894-4117; fax: +1-404-894-8780.

E-mail address: sharafma@yahoo.com (M.A. Sharaf).

0032-3861/02/$ - see front matter
PII: S0032-3861(01)00545-6

plane of the particle and is thus perpendicular to the deformation direction. The opposite is the case for prolate particles, which have their primary axis along the particle that is thus parallel to the direction of deformation. This technique also gives a non-uniform stress field around the particles upon contraction of the elastomer [4–6]. It is possible, of course to design experiments in which the effects of shape changes are separated from the orientation effects, and the non-uniform stress fields are removed. The way to do this would be to dissolve away the host matrix used to prepare the oblate particles, and then randomly blend the particles into another elastomeric matrix.

In the experimental study of relevance here, oblate PS particles covering a range of axial ratios were generated in a poly(dimethylsiloxane) (PDMS) elastomer [6]. Axial ratios were controllable, since they were generally found to be close to the values of the biaxial draw ratio employed in their generation. The moduli of these anisotropic composites were reported, but only in the plane of the biaxial deformation [6]. It was not possible to obtain moduli in the perpendicular direction, owing to the nature of the thin film that had to be used in the experimental design.

There is some literature documenting the specific fact that different filler shapes result in different types of reinforcement, with various anisotropies in mechanical properties [7–10], and a great deal more on reinforcing effects of fillers in general [11–24]. There are a number of ways in which a filler can reinforce an elastomeric network, including increasing the effective degree of cross-linking, amplifying the macroscopically imposed strain, etc. An additional effect of the filler is the imposition of excluded volume effects on the network chains, and this is probably the easiest contribution to simulate [25–29]. The fact that the chains cannot go into the volumes occupied by the filler particles deforms their spatial configurations (relative to the initial reference conformations in the absence of filler). In the case of prolate ellipsoids, the changes can be either expansions or compressions, depending on the lengths of the chains. Since the distributions of end-to-end chain separations are central to the calculation of elastomeric properties [30,31], quantities such as the modulus would change correspondingly. In excluded-volume simulations of this type, one postpones treatment of other effects that contribute to the reinforcement.

Results from small-angle neutron scattering (SANS) and small-angle X-ray scattering (SAXS) studies have provided information on such filler-induced deformations of polymer chains [21,30,32]. The neutron scattering study by Nakatani et al. on silica-filled PDMS is most relevant to the present issues [32]. They found that when the chain dimensions were approximately the same magnitude as the filler particle diameters, the scattering results showed a *decrease* in chain dimensions at all filler concentrations. For longer chains in the presence of fillers at relatively low concentrations, there was an *increase* in these dimensions. These experimental results are in good semi-quantitative agreement with earlier Monte Carlo simulations in which spherical filler particles were placed either (i) regularly on a three-dimensional cubic lattice, or (ii) irregularly, in random arrangements throughout the volume in which the chains were subsequently generated [25–29].

The previous simulations on non-spherical particles by the present authors involved Monte Carlo simulations on prolate particles in a matrix of polyethylene (PE) [33]. The simulations were done for a sufficiently high temperature that the polymer would be amorphous (and thus elastomeric). The particles were placed on a cubic lattice, in part for convenience and in part because it is possible to have particles self assemble into such arrays if they are charged and the composite is aged under the right conditions [34]. In any case, they were axially oriented in a way consistent with their orientation in the composites that had been experimentally investigated. There were found to be particle-induced deformations that corresponded to decreased chain dimensions and radii of gyrations upon insertion of spherical particles amongst the chains, which is consistent with earlier simulations and with the neutron scattering results already mentioned. The decreases in dimensions and radii, however, were subsequently followed by increases upon increasing the axial ratios to distort the spherical particles into prolate shapes. The chain dimensions also became anisotropic, with significant differences parallel and perpendicular to the direction of the particle axes. Use of these distributions in the standard three-chain model of rubberlike elasticity gave the corresponding elongation moduli. The reinforcement from the prolate particles was found to be greatest in the parallel direction, and the changes were in at least qualitative agreement with the corresponding experimental results [33].

The present study is a parallel investigation which considers oblate instead of prolate particles. It first focuses on the distribution $P(r)$ of the end-to-end vector of the network chains [35,36]. The distributions obtained from the simulations are then used in standard rubberlike elasticity theory to estimate moduli within the plane of the disc and perpendicular to it. Finally, at least qualitative comparisons will be made between these simulated moduli and the most relevant experimental results available at the present time.

2. The model and numerical calculations

2.1. The geometry of the model

As in the case of the prolate particles [33], the simulations were carried out for PE chains having $n = 300$ backbone bonds. The simulations were carried out for 425 K, which is above the melting point of PE, so as to model the effects of the particles within an amorphous elastomeric matrix. The anisotropic effects arising from the oblate particles were characterized by covering a range of values of their sizes and aspect (axial) ratios δ (of major to minor axes). For each

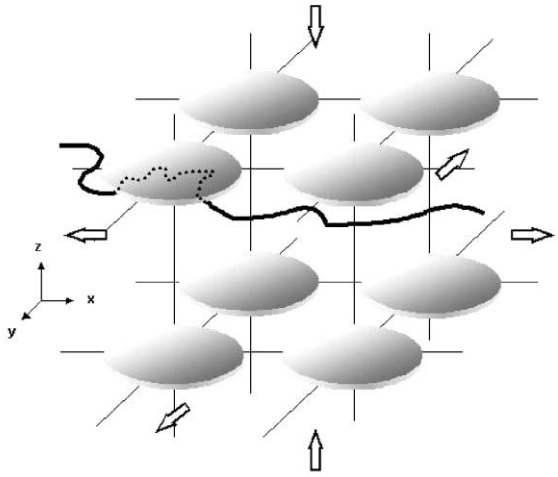

Fig. 1. A three-dimensional cubic lattice of oblate filler particles as they appear after distortion of the spherical particles into aligned oblate shapes. The aspect ratios δ of the ellipsoids were varied by changes in the extent of the extension applied biaxially in the x–y plane, as shown by the arrows. This biaxial extension is equivalent to compression along the particle (z) axis, as illustrated. Also shown is a polymer chain that was randomly generated among the oblate filler particles to determine particle-induced changes on its spatial configurations, and thus on its distribution of end-to-end distances.

simulation, the particles were assumed to be uniform in size and shape, and firmly bonded to the PE matrix. Fig. 1 shows a sketch of the model employed, whereby the originally spherical particles are stretched biaxially into oblate shapes. The particles are arranged on a cubic lattice, and aligned in the direction of the plane of deformation. At the same volume fraction of filler, the unit cell dimensions were varied through the choice of the radius r_{sph} of the initially undeformed spherical filler particles.

A large number of Monte Carlo chains ($N = 30\,000$) was generated to assure that the results were statistically significant. A non-biased sampling was achieved by randomly generating the locations for the origins of the chains, and Euler's rotation matrix was employed in order to have random directions for the generation of chains. van der Waal's radii of the atoms were taken into consideration when checking for overlap between the filler particles and the polymer chain being generated; the CH_2 group was treated as a united atom having a radius $r_{CH_2} = 2.1$ Å. Configurations that resulted in overlaps between the chains and filler particles were rejected, so as to model this excluded volume effect on the chain dimensions and elastomeric properties.

2.2. The Monte Carlo simulations

The Monte Carlo scheme employed here uses a modified Metropolis algorithm to calculate the average $\langle x \rangle$ of an observable variable that depends on the chain configurations [36]. The averaging is over all configurations $\{\phi\}_i$ representing sets of $\{\phi_1, \ldots, \phi_n\}_i$ possible torsional angles along the backbone of a specific chain i with n repeat units. The weighting factor Ω_i for the ith of these is a Boltzman factor defined for a specific configuration $\{\phi\}_i$ as a product of a series of factors $U_{\zeta\eta;k}$, each associated with state ζ for bond angle ϕ_{k-1} and state η for bond angle k [36].

2.3. The rotational isomeric model

According to the rotational isomeric state (RIS) theory, the statistical weights for a polymer chain are given by [37,38]:

$$u_{\zeta\eta} = \exp(-E_{\zeta\eta}/RT) \tag{1}$$

where $E_{\zeta\eta}$ is the energy for a pair of bonds with the first being in state ζ and the second in state η (ζ and η being either *trans*, *gauche*$^+$, or *gauche*$^-$) [33]. These three discrete rotational isomeric states are taken to occur at torsional angles $\phi = 0$, 120, $-120°$, respectively. Specific values used for the energies $E_{\zeta\eta}$ are now standard, and are given elsewhere [33]. It is noteworthy here that Hill and Stepto were the first to employ the conditional probability matrices for generating Monte Carlo chains [39]. Details of the generation of Monte Carlo chains from conditional probability matrices are discussed in greater detail in a number of publications [25–29,33,35,39].

2.4. End-to-end vectors

For each chain configuration, the end-to-end vector $\mathbf{r}$ was calculated in the usual way, by multiplication of bond vectors containing equilibrium bond lengths (1.54 Å for PE) with transformation matrices containing the relevant complementary bond angles of the chain (68.0° for PE) and the rotational angles already cited [25–29,33,35]. The end-to-end distances were obtained from the described Monte Carlo scheme. The range of r/r_{max} was divided into 15 intervals (grids), where the maximum extension r_{max} is given by $n\ell_0$ (for n bonds of length ℓ_0). The radii of gyration as well as the relevant x, y, and z components were obtained in the same manner. The numbers of chains in the various intervals were averaged to give a histogram of the distribution, and a smooth curve was then placed through the points by cubic splines fitting.

2.5. Elastomeric properties

The resulting distribution $P(r)$ can now be used to calculate the desired elastomeric properties of the chains [33,35]. It is directly related to the Helmholtz free energy $A(r)$ of a chain having the end-to-end distance r by:

$$A(r) = c - kT \ln P(r) \tag{2}$$

where c is a constant. This equation can be applied to the case of elongations in which the chains respond affinely (linearly) to the macroscopic deformation [33]. This macroscopic deformation λ_t along the direction t is defined as:

$$\lambda_t = L_t/L_{ot} \tag{3}$$

Here, L_{ot} is the length of the sample in the direction $t(t = x, y, z)$ in the unfilled reference state, and L_t is its value in the filled network at the start of the experiment. Assuming an affine deformation, L_{ot} and L_t are related to the t components of the end-to-end vector of the chains. The three main-axis deformation tensor components λ_{it} are related to the volume at the start of the experiment V, and the reference volume V_o of the isotropic unfilled network by:

$$\lambda_{ix}\lambda_{iy}\lambda_{iz} = V/V_o \tag{4}$$

Since in this study anisotropy is induced only along the direction of the deformation, it follows that two of the three terms are equivalent. As would be expected, $V \neq V_o$ due to the anisotropy of the polymer chains induced by the oriented filler particles. The deformation ratio α_t relative to the dimension L_t at the start of the experiment is given for the case of isotropic deformation by:

$$\alpha_t = L_t/L_{it} = (V/V_o)^{-1/3}\lambda_t \tag{5}$$

For anisotropic deformations

$$\alpha_t = L_t/L_{it} = (L_{it}/L_{ot})^{-1}\lambda_t = (\lambda_{it})^{-1}\lambda_t \tag{6}$$

where λ_{it} refers to the change of dimensions of the filled network relative to the unfilled network before application of the deformation. Incompressibility of the network is assumed, so the volume V remains constant after the stress is applied. When the deformation α is applied along the draw direction of the filler particles, for example the z-axis,

$$\lambda_z = (\lambda_{iz})\alpha \qquad \lambda_x = \lambda_y = (\lambda_{ix})\alpha^{-1/2} \tag{7}$$

Whereas if the direction of deformation is in the perpendicular direction x or y, three independent deformation ratios will result.

$$\lambda_x = (\lambda_{ix})\alpha \qquad \lambda_y = (\lambda_{ix})\alpha^{-1/2} \qquad \lambda_z = (\lambda_{iz})\alpha^{-1/2} \tag{8}$$

Within these approximations, the three-chain model leads to the following general expression for the elastic free energy change during deformation [33,35]:

$$\Delta A = (\nu/3)[A(r_o\lambda_x) + A(r_o\lambda_y) + A(r_o\lambda_z - 3A(r_o)] \tag{9}$$

where, ν is the number of mols of chains in the network and $r_o = \langle r^2\rangle_o^{1/2}$ is the value of the root-mean-square (rms) end-to-end vector of the chains.

The nominal stress f^* (defined as the elastic force at equilibrium per unit cross-sectional area of the sample in the undeformed state) can be obtained from [40]:

$$f^* = -T\left(\frac{\partial \Delta A}{\partial \alpha}\right)_T \tag{10}$$

For stretching parallel to the draw direction, this becomes:

$$f^* = -(\nu kTr_o/3)[G'(r_o(\lambda_{iz})\alpha) - \alpha^{-3/2}G'(r_o(\lambda_{ix})\alpha^{-1/2})] \tag{11}$$

and for deformation transverse to the draw direction, e.g. along the x-axis,

$$f^* = (-\nu kTr_o/3)[G'(r_o(\lambda_{ix})\alpha) - \alpha^{-3/2}/2\{G'(r_o(\lambda_{iz})\alpha^{-1/2}) + G'(r_o(\lambda_{iy})\alpha^{-1/2})] \tag{12}$$

where $G(r) = \ln P(r)$, and $G(^{\prime}r)$ denotes the derivative dG/dr. The IMSL subroutine 'CSDER' was used in the numerical calculations of the derivative of the smoothed function P' (r/r_{max}), together with the relationship $G' = P'/P$.

The modulus or reduced stress defined as [40]:

$$[f^*] = \frac{f}{\alpha - \alpha^{-2}} \tag{13}$$

is often fitted to the Mooney–Rivlin semi-empirical formula [40]

$$[f^*] = 2C_1 + 2C_2\alpha^{-1} \tag{14}$$

where $2C_1$ and $2C_2$ are constants independent of deformation α. Some of the results obtained will be represented in this form.

In the case of filled networks, however, the deformation α relevant to the elastomeric matrix chains should be replaced by an effective mean amplified extension ratio α_{eff} due to the hydrodynamic effects of the filler, i.e. the disturbance of the strain distribution [31,41]:

$$\alpha_{eff} = (\alpha - 1)X_{eff} + 1 \tag{15}$$

where the effective 'Guth amplification factor' X_{eff} for spherical particles is [31,41]:

$$X_{eff} = 1 + 2.5v_f + 14.1v_f^2 \tag{16}$$

For non spherical particles ($\delta > 1$), X_{eff} is given by [41]:

$$X_{eff} = 1 + 0.67\delta v_f + 1.62\delta^2 v_f^2 \tag{17}$$

where v_f is the volume fraction of filler. As already mentioned, δ is the aspect ratio shape factor, which for oblate particles is the ratio of the diameter to the thickness of the filler particles.

3. Results and discussion

3.1. Radial distributions

The Monte Carlo results obtained for the rms end-to-end distances $\langle r^2\rangle_o^{1/2}$ are reported in Table 1. They are for both the initially undeformed spherical particles and those deformed into oblates with their particle axis oriented along the z-axis, transverse to the plane of deformation of the particles, as shown schematically in Fig. 1.

Figs. 2 and 3 show the distributions of the end-to-end vector $P(r)$ as a function of the relative extension r/r_{max} for PE chains at a volume fraction of filler $v_f = 0.2$. The results are for particles that were initially undeformed spheres (aspect or axial ratio $\delta = 1$) with radii of 20 and

Table 1
Results of Monte Carlo calculations for polyethylene chains having 300 skeletal bonds in a cubic lattice of oriented oblate filler particles, at 425 K and at a volume fraction of filler $v_f = 0.2$

δ[a]	a[b]	$\langle r^2\rangle_o^{1/2}$[c]	$\langle s^2\rangle_o^{1/2}$[d]	C_8[e]	λ_{iz}[f]	$\lambda_{i,x,y}$[g]
$r_{sph} = 20$ Å						
0.0	55.13	71.15	49.76	6.76	1.0	1.00
1.0		61.22	43.45	5.00	1.0	1.00
2.0		58.54	41.60	4.58	0.64	1.04
4.0		57.57	41.05	4.43	0.45	1.06
6.0		57.64	41.26	4.44	0.44	1.06
$r_{sph} = 40$ Å						
0.0	110.25	71.15	49.76	6.76	1.00	1.00
1.0		65.36	46.37	5.68	1.00	1.00
2.0		64.36	45.75	5.53	0.84	1.05
4.0		62.92	45.06	5.29	0.74	1.05
6.0		63.14	45.23	5.32	0.73	1.06

[a] Aspect ratio of the oriented oblate particles.
[b] Cubic unit cell dimension in Å.
[c] Root-mean-square end-to-end distance in Å.
[d] Root-mean-square radius of gyration in Å.
[e] Characteristic ratio, $\langle r^2\rangle_o/n\ell^2$.
[f] Anisotropic changes of initial chain dimensions relative to the spherical ones in the longitudinal direction of the oriented particles (z axis).
[g] Anisotropic changes of initial chain dimensions relative to the spherical ones in the transverse direction of the oriented particles (x,y axes).

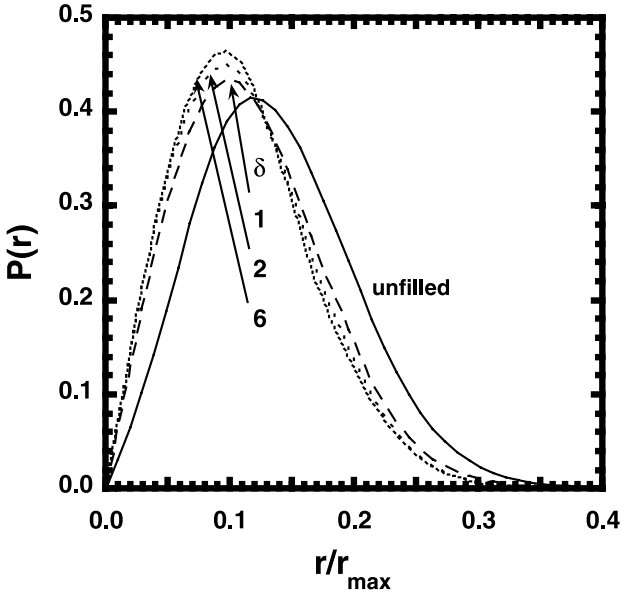

Fig. 2. Radial distributions $P(r)$ of the end-to-end vector $\mathbf{r}$, obtained by Monte Carlo simulations, shown as a function of the relative chain extension r/r_{max}. In this figure and the following ones, the results pertain to amorphous polyethylene chains having $n = 300$ skeletal bonds, at 425 K, in the presence of oriented oblate filler particles having a volume fraction v_f of 0.2. The quantity r_{sph} denotes the radius of the filler particle before its deformation into oblate shapes having the specified values of the aspect ratio δ The particular results shown here correspond to $r_{sph} = 20$ Å, and the solid line represents the results for the unfilled polymer chain (in the absence of any particles).

40 Å, respectively. Calculations were also carried out for oblate ellipsoidal particles which had $\delta = 0.5$, 0.25, 0.166, and 0.125. For purpose of clarity, only representative results are shown in these two figures. Each curve is labeled with the appropriate value of δ, and results for free chains (in the absence of filler particles) are represented by the solid line. The chains in the lattice of spherical particles clearly show a shift to lower values of r/r_{max}, which is a clear indication that the chains are compressed relative to the free chains. A characteristic feature of Figs. 2 and 3 is the fact that drawing the spherical filler particles into oblate ones causes a further shift to relatively lower values of r/r_{max}, with the chain dimensions being decreased. This could easily be described in terms of the preferential orientation of the chains in the plane of deformation that is perpendicular to the particle axis, thus resulting in a preferential decrease in the effective free volume in the biaxial deformation plane. As the draw ratio increases in the plane, the chains become restricted in the biaxial deformation plane and are not able to extend in the z-direction (which is becoming more and more filled by the expanding disk-shaped oblate particles). This is in contrast to the behavior observed in the case of cigar shaped prolate particles, specifically a shift to higher values of r/r_{max}, i.e. towards those for the unfilled chains [33]. This has been already described in terms of the preferential orientation of the chains that occurs along the draw direction, resulting in a preferential increase of the effective free volume in the same directions. Thus the chain dimensions would have been expected to increase.

Fig. 3 presents a clear demonstration of the effect of the filler particle size on these changes. The magnitude of the observed shift for $r_{sph} = 40$ Å as the aspect ratio δ of the spheres decreases is far less than that observed for the smaller filler particles (20 Å). Such differences are expected

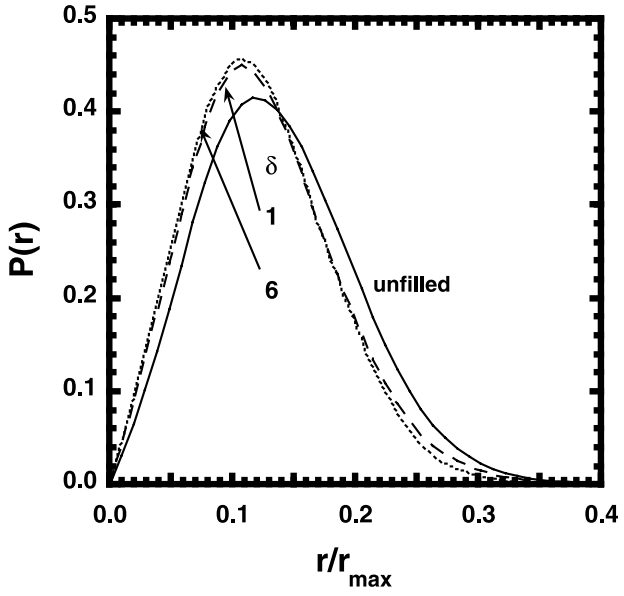

Fig. 3. Radial distributions for the case $r_{sph} = 40$ Å. See legend to Fig. 2.

as a result of an increase of the lattice unit cell dimensions with an increase in particle size, when the volume fraction of the filler is kept constant, as shown in Table 1. With an additional increase in the free volume accessible to the chains, this is accounted for by the anisometry of particle shape effects resulting from the spheres pre-strained into oblate particles. This clearly demonstrates the effects of the particle shape on the matrix polymer chains.

Of course, in both Figs. 2 and 3 all the curves for a chain in a matrix filled with spherical or oblate particles display significant deviations from that for the free chains, and from Gaussian behavior in general. In other words, when the cubic unit cell dimension are greater than the root-mean-square end-to-end distance $\langle r^2\rangle_o^{1/2}$ of the polymer chains, the effects of the volume exclusion by the filler particles become less and less important. In the case of oblate filler particles, the excluded volume effects should be taken into consideration with the decrease in the aspect ratio if the spherical particles are biaxially stretched (or compressed) into oblate ones, when both the particle size and volume fractions are the same. As is readily apparent, there is a decrease in the effective free volume preferentially accessible to the chains, with a decrease in the aspect ratio, as a result of anisotropic particle shapes [33].

Unique distributions would be expected if the simulations were extended to lattices with $r_{sph} < 20$ Å. Unfortunately, most of the generated chain conformations then overlap with filler particles and have to be rejected, and the computer time needed for such simulations becomes unacceptably long.

3.2. End-to-end dimensions and radii of gyration

For purposes of illustration, Fig. 4(a) presents values of the rms end-to-end distance as a function of the reciprocal aspect ratio $1/\delta$ with $1/\delta = 0$ corresponding to the unfilled material. The results show that $\langle r^2\rangle_o^{1/2}$ for chains in lattices with spherical and oblate particles are significantly reduced in comparison to those in unfilled lattices. Again, as expected, values of $\langle r^2\rangle_o^{1/2}$ for filler particles having initial $r_{sph} = 40$ Å are higher than those for spherical particles with initial $r_{sph} = 20$ Å. These differences are expected as a result of an increase in the unit cell dimensions for a fixed value of v_f. Most important, the results clearly demonstrate the effects of anisotropic shapes on the distributions of the end-to-end vectors. Spheres, which are pre-strained into anisotropic oblate shapes lead to a decrease in the effective free volume accessible within a unit cell, or could even permit the chains to extend into neighboring cells, anisotropically, in the direction of draw. In other words, excluded volume effects are now not negligible for such anisotropic disk-shaped oblate particles, in contrast to the case of the cigar shaped prolates [33].

In Fig. 4(b), the rms radii of gyration are displayed as a function of $1/\delta$. As shown here and in Table 1, the radii of gyration $\langle s^2\rangle_o^{1/2}$ and characteristic ratios $\langle r^2\rangle_o/n\ell_o^2$

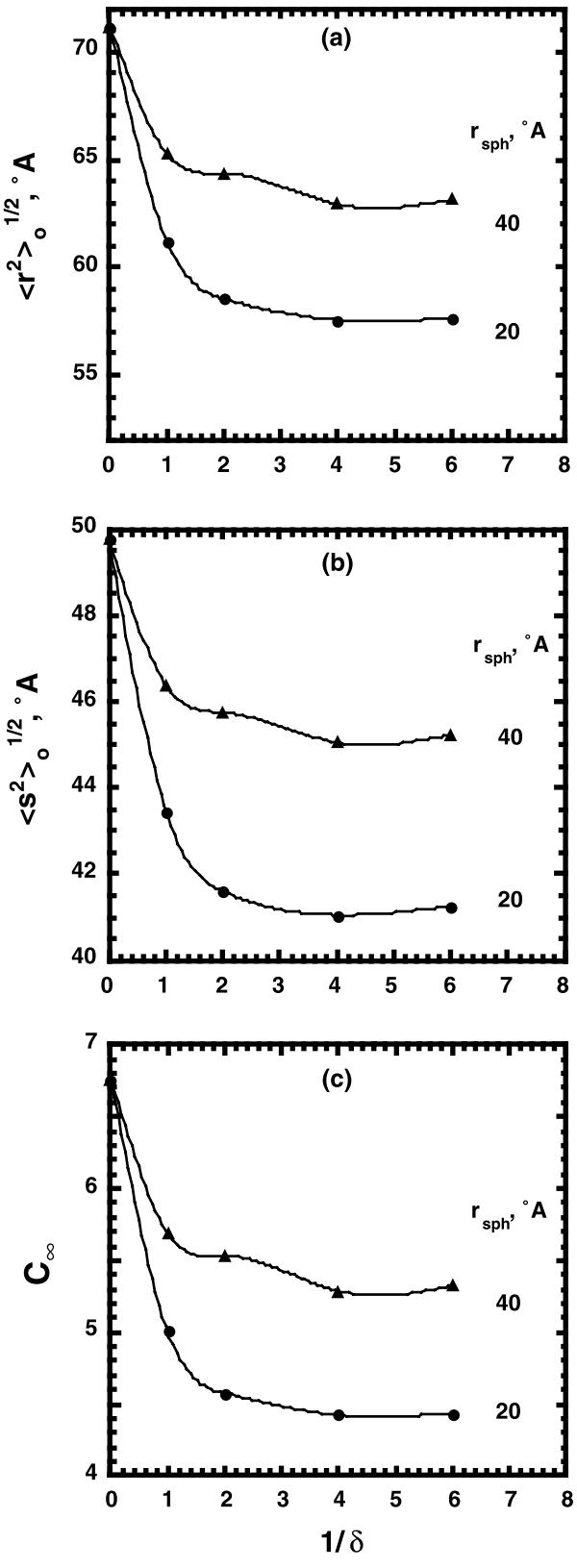

Fig. 4. Root-mean-square end-to-end distances (a), the root-mean-square radii of gyration (b), and the characteristic ratio (c) of the chains described in Figs. 2 and 3 as a function of the reciprocal aspect ratio $1/\delta$ for filler particles having $r_{sph} = 20$ or 40 Å. See legend to Fig. 2.

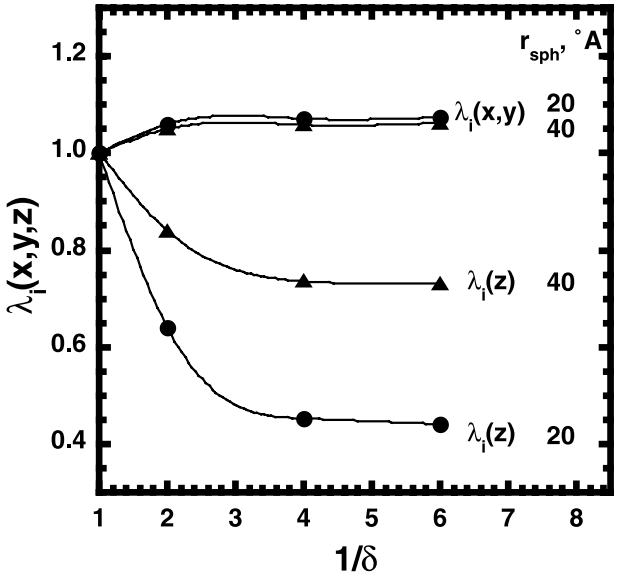

Fig. 5. Anisotropic changes of the initial chain dimensions induced by the aligned oblate particles relative to the dimensions in the presence of the spherical particles ($\delta = 1.0$). The results are shown as a function of the reciprocal aspect ratio $1/\delta$ for filler particles having $r_{sph} = 20$ or 40 Å. Results are presented for the longitudinal direction of the particle axes (z direction), and for the transverse (x, y) plane in the direction of biaxial deformation of the initial spherical particles. See legend to Fig. 2.

(illustrated in Fig. 4(c)) are found to follow the same trends seen in Fig. 4(a).

3.3. Changes in the components of the end-to-end dimensions

The effects of the anisotropic shape on the distribution functions of the chains are shown in Fig. 5 and Table 1. The anisotropic changes in the chain dimensions of the pre-strained oblate filled matrix relative to the spherical one were calculated in the longitudinal and transverse directions of the particle axis. Values of $\lambda_{it} = L_{it}/L_{ot}$ $(t = x, y, z)$ serve as a measure of the change of dimensions of the network filled with pre-strained oblate particles relative to the spherical one, before the application of the deforming strains. These values are represented in Fig. 5 as a function of the reciprocal aspect ratio for oblate filler particles having $r_{sph} = 20$ or 40 Å. Of significance here are the observed pronounced decreases in chain dimensions along the particle (z) axis. This is consistent with conjectures reached in the previous section about the effective free volume accessible to the chain in the presence of this particular disk-shaped oblate particle in the matrix. Undoubtedly, there is anisotropy in the initial dimensions of the chain as a result of the anisotropy of the pre-stretched oriented filler particles in the x–y plane of the draw. Along the direction of particle (z) axis, the initial dimensions of the chain were only slightly affected and reached asymptotic values with increase in the reciprocal aspect ratio $1/\delta$. The effects are even larger when such values are calculated relative to the unfilled networks.

This clearly underscores the fact that composites having non-spherical oriented filler particles demonstrate discernible anisometry. Consequently, significant changes in the deformation behavior are expected, as will be addressed in the following sections. It is now apparent that such excluded volume effects of oriented particles result in anisotropic particle-induced chain deformation (a type of 'overstrain'). In consequence, stiffening of the polymeric matrix upon addition of hard fillers is expected owing to larger microscopic than macroscopic strains. As such, chain dimensions are generally smaller relative to those in a matrix filled with prolate particles having the same initial size of the sphere at equivalent extents of distortion of the particles [33]. This is a clear reflection that the larger planar size of the disk shaped oblate particles severely reduces the effective free volume accessible to the chains. Consequently, the chains are forced to adopt more compressed configurations, in particular along the particle (z) axis.

3.4. Transverse (planar) moduli and overstrain

Fig. 6(a) and (b) demonstrate the anisotropic shape effects of the oriented filler particles on the reduced modulus $[f^*]/\nu RT$ as a function of reciprocal elongation α^{-1}. The representation is that suggested by the Mooney–Rivlin relationship [40], and the results are for the chains described in Figs. 2 and 3. Contrary to the case of chains in a matrix of oriented prolate particles, there are no pathological maxima and minima observed earlier in some stress–strain curves [33]. Such pathological behavior indicated that a slight change in the shape of the distribution function near r_o had a pronounced effect on the stress–strain behavior. The effect might also be related to the histogram method generally employed. The proper calculation of the distribution function near r_o might require histograms with smaller intervals around r_o. In the earlier case, the fact that the range of r/r_{max} was divided into only 15 intervals could have been responsible for at least part of the observed behavior.

In any case, at small strains an increase in the normalized longitudinal modulus in the x–y plane of draw of the particle is seen in Fig. 6(a) for chains filled with oriented oblate particles. The increases are relative to that for the free chain and matrix chains filled with spherical particles ($r_{sph} = 20$ Å). The enhancement of the small-strain modulus was estimated to be 400–600%. Similar behavior is observed in Fig. 6(b) for matrices filled with larger particles ($r_{sph} = 40$ Å). All the isotherms in these figures show upturns in modulus as elongation increases, and such non-Gaussian behavior is clearly a result of the finite extensibility of the chains. More specifically, these upturns are due to the rapidly diminishing number of configurations at larger values of the end-to-end separation r. Correspondingly, this is accompanied by significant decreases in the entropy of the chains, with corresponding increases in $[f^*]$. Such increases

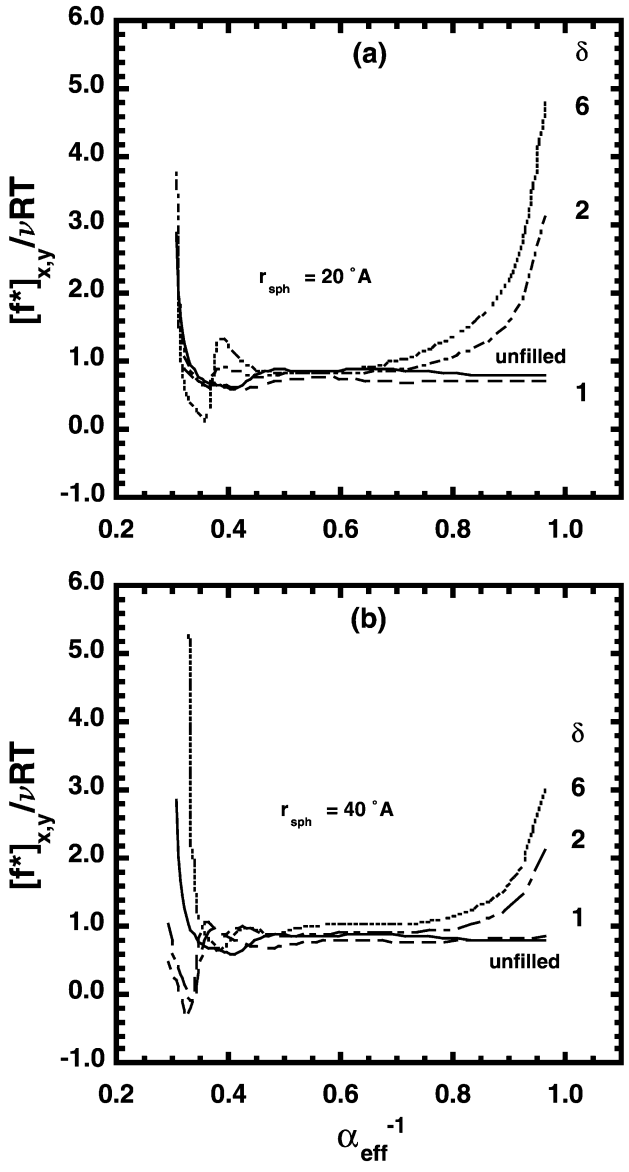

Fig. 6. Normalized moduli in the x–y plane of biaxial extension of initial spherical particles into oblate shapes having the specified value of the aspect ratio δ shown as a function of the reciprocal effective elongation α_{eff}^{-1} for the case $r_{\text{sph}} = 20$ Å (a) and for $r_{\text{sph}} = 40$ Å (b) See legend to Fig. 2.

are more pronounced for particles having smaller aspect ratios, e.g. $\delta = 0.166$ (larger dimensions in the x–y plane of drawing).

Anisotropic increases in modulus $[f^*]_{x,y}$ in the biaxial plane of draw above those for the free chains are clearly present, particularly at small strains. An increase in particle size results in an increase in the unit cell dimensions, at fixed υ_f. As is demonstrated in Fig. 6(a) and (b), and as expected from Figs. 2 and 3, chains in lattices of oriented non-spherical oblate particles also show nearly equal elongations at which the upturns in the modulus occur. This is a result to be expected from the diminished values of r_o. Again, with increase in particle size (i.e. with increasing unit cell dimension at fixed υ_f), the nominal stress for large aspect ratios approaches the limit of a free chain. In this connection, it is noteworthy that the stress–strain behavior depends on the specific shape of the end-to-end distribution function near r_o [33,35].

Deviations from the Mooney–Rivlin predictions can easily be due to slight changes in the shape of the distribution function near r_o [33,35]. In our previous study on spherical particles arranged on a cubic lattice it was found that even at equivalent values of r_o, the shapes of the stress–strain curves were entirely different, with some showing some unphysical behavior in a manner similar to that seen in Fig. 6 at higher elongations. It is well accepted that upturns in the modulus should occur earlier for filled chains owing to their induced overstrains in the initial state. Such effects are not clearly discernible, however.

The main point here is that the planar (transverse) moduli obtained for chains in oriented oblate particle lattices with undeformed $r_{\text{sph}} = 20$ and 40 Å are larger than those for unfilled and networks filled with spherical particles, in particular at low extensions. Furthermore, it is clear that a slight change in the particle size, and correspondingly in the unit cell dimensions, has significant effects on values of the modulus. It should be noted that for Gaussian chains the modulus $[f^*]/\nu RT$ is independent of elongation, and has a value of unity. Fig. 6(a) and (b) show that PE chains having 300 bonds in an unfilled network and even in some of the filled networks have almost Gaussian-like behavior at low elongations.

The results obtained clearly demonstrate the extent to which excluded volume effects of oriented non-spherical particles result in particle-induced chain deformations that are anisotropic. This is certainly a type of strain amplification 'overstrain'. In consequence, higher values of moduli are expected as a result of the stiffening of the polymeric matrix chains. This is a result of the addition of hard fillers making the microscopic strains larger than the macroscopic strains.

3.5. Longitudinal moduli

Fig. 7(a) and (b) show the longitudinal moduli, along the direction of the particle (z) axis. As would be expected, at lower values of the axial ratio of the oblate particles, values of the modulus are below that for chains in unfilled matrices. The deviation becomes less pronounced with decrease in δ however. It is worth noting that a decrease in the aspect ratio of the oriented particles is expected to change the effective lateral dimensions accessible to the chain. In particular, chain dimensions undergo a pronounced decrease along the particle axis. Hence, there are decreases in the longitudinal moduli with decreases in the aspect ratio of the oriented oblate particles. This would be expected as a result of a reduction in the effective free volume that very significantly decreases values of the longitudinal (z) components of r_o, as already discussed.

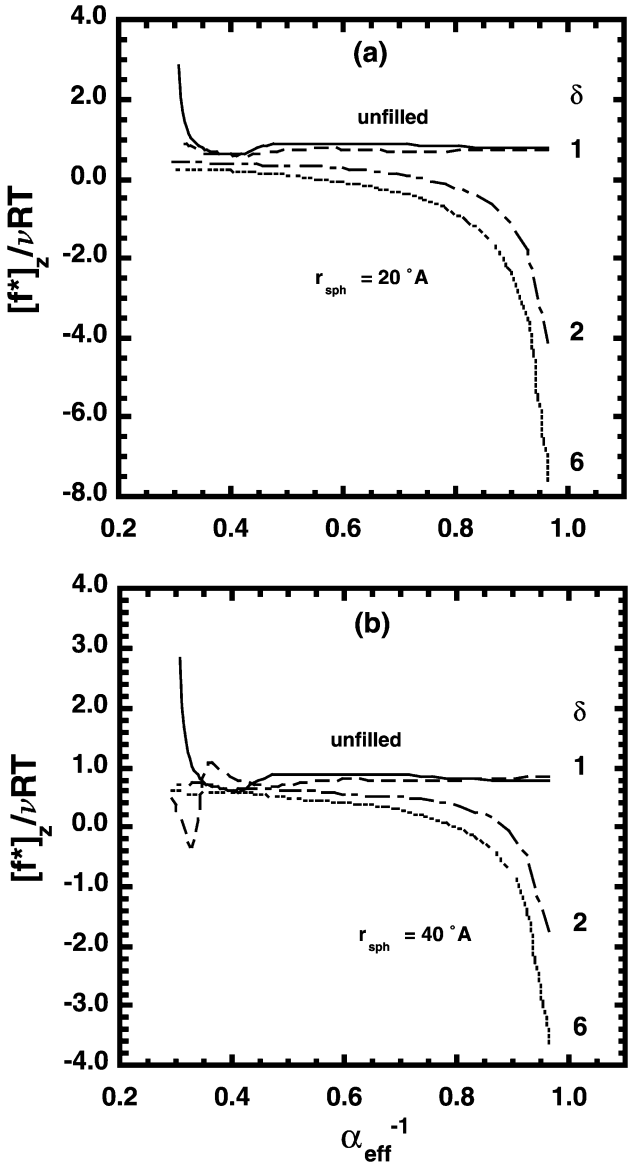

Fig. 7. The comparisons made in Fig. 6, but now for the moduli along the direction of the longitudinal particle (z) axis for the case $r_{sph} = 20$ (a) and for $r_{sph} = 40$ Å (b).

As before, the stress–strain behavior at the same loading υ_f shows strong dependences on the sizes and axial ratios of the particles.

3.6. Some comparisons with experiment

The numerical results thus presented are in qualitative agreement with changes in moduli experimentally obtained by Wang et al. [6] for the case of oriented rigid oblate PS particles prepared by biaxial deformations above the PS glass transition temperature. Unfortunately, it was not possible to obtain moduli perpendicular to the disks, owing to the nature of the thin film that had to be used in the experimental approach taken. Also, quantitative comparisons are difficult because the polymers are different, there are non-uniform stress fields around the particles after the deforming matrix is allowed to retract, and the present simulations apply to the particles on an ideal cubic matrix. Additional experiments and simulations should permit more detailed comparisons between experiment and theory.

Acknowledgements

It is a pleasure to acknowledge the financial support provided JEM by the National Science Foundation through Grants DMR 00-75198 (Polymers Program, Division of Materials Research) and by the Dow Corning Corporation. The authors are also grateful for the financial support provided by the Foundation through grant INT 96-05191 (US-EGYPT International Program).

References

[1] Kraus G. Adv Polym Sci 1971;8:155.
[2] Boonstra BB. Polymer 1979;20:691.
[3] Saam JC. Mat Res Soc Symp Proc 1992;91:274.
[4] Wang S, Mark JE. Macromolecules 1990;23:4288.
[5] Nagy M, Keller A. Polym Commun 1989;30:130.
[6] Wang S, Xu P, Mark JE. Macromolecules 1991;24:6037.
[7] Beuche AM. J Polym Sci 1957;25:139.
[8] Chow TS. J Polym Sci, Polym Phys Ed 1978;16:959.
[9] Wu T. Int J Solids Struct 1966;2:1.
[10] Ahmed S, Jones FR. J Mater Sci 1990;25:4933.
[11] Edwards CJ. Mater Sci 1990;25:4175.
[12] Wang M-J. Rubber Chem Technol 1998;71:520.
[13] Vidal A, Donnet JB. Prog Colloid Polym Sci 1987;75:201.
[14] Medalia AI. Rubber Chem Technol 1987;60:45.
[15] Maier P, Goeritz D. Kautsch Gummi Kunstst 1996;49:18.
[16] Cohen Addad JP. Polymer 1992;33:13.
[17] Jones DAR, Leary B. J Colloid Interface Sci 1971;147:479.
[18] Payne AR, Whittaker RE. Rubber Chem Technol 1971;44:440.
[19] Witten TA, Rubinstein M, Colby RH. J Phys II 1993;3:367.
[20] Mullins L. Rubber Chem Technol 1969;42:339.
[21] Rharbi B, Cabane A, Vacher M, Joanicot M, Boue F. Europhys Lett 1999;46:472.
[22] Oberdisse J, Rharbi Y, Boue F. Comp Theor Polym Sci 2000;10:207.
[23] Wu D, Hui K, Chandler D. J Chem Phys 1992;96:835.
[24] Gusev A, Rozman MG. Comput Theor Polym Sci 1999;9:335.
[25] Sharaf MA, Kloczkowski A, Mark JE. Comp Polym Sci 1994;4:29.
[26] Yuan W, Kloczkowski A, Mark JE, Sharaf MA. J Polym Sci, Part B: Polym Phys 1996;34:1647.
[27] Kloczkowski A, Sharaf MA, Mark JE. Comp Polym Sci 1993;3:39.
[28] Kloczkowski A, Sharaf MA, Mark JE. Chem Engng Sci 1994;49:2889.
[29] Sharaf MA, Kloczkowski A, Mark JE. Polym Preprints 1995;362:368.
[30] Westermann S, Kreitschmann M, Pyckhout-Hintzen W, Richter D, Straube E, Farago B, Goerigk G. Macromolecules 1999;32:5793.
[31] Heinrich G, Vilgis TA. Macromolecules 1993;26:1109.
[32] Nakatani AI, Chen W, Schmidt RG, Gordon GV, Han CC. Polymer 2001;42:3713.
[33] Sharaf MA, Kloczkowski A, Mark JE. Comput Theor Polym Sci 2001;11:251.
[34] Pu Z, Mark JE, Jethmalani JM, Ford WT. Chem Mater 1997;9:2442.
[35] Curro JG, Mark JE. J Chem Phys 1984;80:4521.
[36] Curro JG, Schweizer KS, Adolf D, Mark JE. Macromolecules 1984;80:4521.

[37] Flory PJ. Statistical mechanics of chain molecules. New York: Wiley, 1969.
[38] Mattice WL, Suter UW. Conformational theory of large molecules. New York: Wiley-Interscience, 1994.
[39] Hill JH, Stepto RFT. Trans Faraday Soc 1971;67:3202.
[40] Erman B, Mark JE. Rubberlike elasticity. A molecular primer. New York: Wiley, 1988.
[41] Guth E. J Appl Phys 1945;15:20.